Research on Engineering Structures & Materials
www.jresm.org
MIM Research Group

Research Article

Wavelet signal analysis for the detection of sand excess defects in hardened concrete

Mohammed Dahmani [*,1,a], Ahcene Arbaoui[1,b], Billel Rebai [2,c]

[1]*Department of Civil Engineering, Faculty of Applied sciences, University of Bouira, 10000, Bouira, Algeria*
[2]*Faculty of Sciences & Technology, Civil Engineering Department, University Abbes Laghrour, Khenchela, Algeria*

Article Info

Article History:

Received 09 Mar 2025

Accepted 10 June 2025

Keywords:

Batching fault;
Excess sand; Concrete;
Wavelet signal analysis;
Ultrasound signals

Abstract

Excessive sand in concrete undermines structural integrity by increasing porosity and reducing durability, necessitating non-destructive quality control methods. This study introduces a wavelet-based approach using discrete wavelet transform multi-resolution analysis (DWT-MRA) to detect sand excess defects. Cylindrical specimens (16×32 cm) of reference concrete (350 kg/m^3 cement) and sand-excess concrete (30% surplus sand) were analyzed via ultrasonic testing (Pundit PL-200), with signals processed in MATLAB. Results identified distinct patterns: reference concrete showed stable signals (70% in categories C1–C4), while sand-excess specimens exhibited anomalies (60% in C7–C10) linked to interfacial defects and porosity. Signal decomposition revealed longitudinal amplitude spikes and transverse attenuation in defective samples, correlated with wavelet coefficients. Recurring values (-32.640/32.624 vs. 31/47) served as diagnostic markers, validated through redundancy analysis. The method's computational efficiency, bypassing machine learning, enables real-time defect detection, offering a scalable, non-destructive solution for structural health monitoring and quality assurance in concrete production.

1. Introduction

Concrete is a heterogeneous material composed of a mixture of aggregates, sand, and paste (cement, water). This material is a key element in our living environment, and due to its durability, mechanical performance, ease of manufacture, and use, it is widely utilized in the construction of various building structural elements in different geometric shapes. Rebai et al. [1]. As a result, concrete has become one of the most economically significant and extensively used materials globally.

Research on concrete properties and non-destructive testing (NDT) methods has evolved significantly. Kovler and Roussel [2] comprehensively analyzed the physicochemical and mechanical properties of fresh and hardened concrete, emphasizing factors influencing workability, strength, and durability. Pedram et al. [3] experimentally evaluated heat transition mechanisms in concrete with subsurface defects using infrared thermography, demonstrating its efficacy in detecting voids and delaminations. Joshaghani and Shokrabadi [4] explored ground-penetrating radar (GPR) applications in concrete pavements, highlighting its utility for thickness measurement and rebar detection. Schabowicz [5] reviewed NDT techniques (ultrasonic, radiographic) for material characterization in civil engineering, stressing their role in quality assurance. Lin et al. [6] developed empirical models to predict ultrasonic pulse velocity (UPV) in concrete, correlating it with compressive strength and mix parameters. Kogbara et al. [7] assessed NDT methods for LNG containment concrete, identifying thermal and mechanical performance criteria for cryogenic environments.

*Corresponding author: mo.dahmani@univ-bouira.dz
[a]orcid.org/0009-0004-2200-9580; [b]orcid.org/0009-0006-1714-9225; [c] orcid.org/0000-0003-3739-2784
DOI: http://dx.doi.org/10.17515/resm2025-735ma0309rs

Advances in signal processing and machine learning have enhanced defect detection. Ouahabi [8] introduced multiresolution analysis (MRA) frameworks for signal and image processing, laying the groundwork for wavelet-based applications. Arbaoui et al. [9] combined wavelet MRA with deep learning to detect and monitor concrete cracks, achieving high accuracy through hierarchical feature extraction. Guo et al. [10] reviewed wavelet analysis applications, emphasizing its advantages in denoising, feature extraction, and multi-scale data interpretation. Further, A hybrid deep learning system based on wavelets was proposed by Arbaoui et al. [11] for real-time crack monitoring and was validated through case studies focused on structural health monitoring. This system was developed following ultrasonic testing conducted on cylindrical specimens measuring 16×32 cm, prepared in accordance with current standards [12-14]. In the present study, MATLAB software [15] will be used to perform a detailed decomposition and analysis of ultrasonic signals, using the same type of specimens.

Recent studies have advanced non-destructive testing and computational methods for material analysis. Hashmi et al. [16-17] proposed models using ultrasonic pulse velocity (UPV) and rebound hammer number (RHN) to estimate age-dependent compressive strength of low-calcium fly ash concrete, demonstrating UPV's reliability over RHN for high fly ash content. Kang et al. [18] introduced a 3D multi-resolution CNN for super-resolution MRI reconstruction, leveraging structural similarities between T1w and T2w images to enhance edge details. Arbaoui et al. [19] combined wavelet-based multiresolution analysis with CNNs to detect concrete dosage defects using ultrasound signals. Luo et al. [20] developed a Mallat algorithm-based system for detecting broken wire rope strands in hanging baskets, utilizing wavelet denoising for stable signal analysis. Mandala et al. [21] optimized atrial fibrillation detection by evaluating Daubechies wavelet basis functions and decomposition levels in ECG signal processing. Machorro-Lopez et al. [22] correlated acoustic emission signals processed with wavelet transforms to structural damage stages in concrete beams. Hu et al. [23] integrated wavelet packet transform with GA-BPNN to classify concrete defects via ultrasonic signals, achieving 91.33% accuracy. Mousavi et al. [24] employed variational mode decomposition and machine learning to assess tree health using ultrasonic data, achieving 100% lab accuracy.

Further research focuses on material composition and durability. Amriou et al. [25] analyzed gravel-sand ratios in concrete, linking increased gravel content to higher strength and lower porosity. Borisiuk and Kochenkova [26] evaluated sand grades' effects on sand concrete properties, emphasizing reduced voidness for improved structural performance. Lee [27] reviewed physicochemical mechanisms driving concrete degradation, highlighting water's role in freeze-thaw cycles, chloride penetration, and corrosion. Sahni and Bashar [28] studied waste foundry sand as a natural sand substitute, noting reduced workability but comparable strength at ≤30% replacement. Jadhav et al. [29] compared river and crushed sand in M30 concrete, observing consistent strength gain with river sand despite initial lower workability. Advanced ultrasonic techniques will be developed to non-destructively quantify porosity gradients in functionally graded materials (FGMs), enabling real-time monitoring of microstructural evolution and enhancing predictive models for performance optimization in critical engineering applications. [30-32].

This study addresses this challenge by proposing a discrete wavelet transform (DWT)-based multi-resolution analysis (MRA) framework to detect sand excess defects in concrete. Cylindrical specimens (16×32 cm) of reference (350 kg/m^3 cement) and sand-excess (30% surplus sand) concrete were analyzed using ultrasonic testing (Pundit PL-200). Signals were decomposed via Daubechies wavelets in MATLAB, isolating defect-specific features through approximation and detail coefficients. Results demonstrate that sand-excess concrete exhibits 60% dominance in categories (C7–C10), longitudinal amplitude spikes, and transverse attenuation, correlating with porosity and interfacial defects. By enhancing sensitivity to compositional deviations, this methodology advances preemptive quality assurance, reducing reliance on destructive testing while aligning with industrial demands for sustainable, high-precision construction practices.

2. Materials and Methods

The methodology of this study was structured into three phases to establish a comprehensive database for identifying concrete composition defects. First, cylindrical specimens (16 × 32 cm) were prepared using two concrete mixes: a standard formulation with 350 kg/m^3 cement content and a defective mix incorporating a 30% excess sand content. Second, Non-Destructive Testing (NDT) was conducted using ultrasonic probes to acquire transverse and longitudinal signals, which were systematically recorded, categorized, and stored. Finally, the acquired signals were processed through wavelet-based multi-resolution analysis (MRA) using MATLAB software to extract defect-specific features and enhance classification accuracy.

Fig. 1 illustrates the methodological workflow encompassing specimen preparation, ultrasonic testing, signal acquisition, wavelet decomposition, and statistical analysis to detect sand excess defects in concrete.

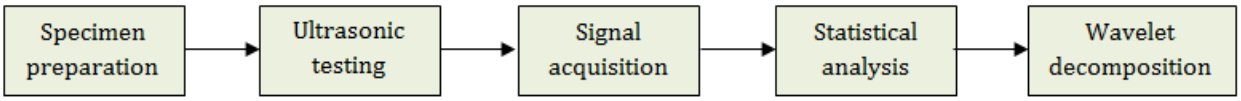

Fig. 1. Methodological workflow

2.1 Preparation of Specimens

Cylindrical concrete specimens were produced in accordance with current standards [12, 13] through five key stages: material selection and preparation, dosing and mixing, pouring, curing, and final grinding. The following constituents were utilized in the fabrication of test specimens:

- Fine Sand "BOUSSAADA" (FSB);
- Washed Crushed Sand 0/4 "SARL ETPHB TAMRAF" (WCS);
- Crushed Gravel (CG) 3/8 "SARL MEZIANE";
- Crushed Gravel (CG) 8/15 "SARL MEZIANE";
- Crushed Gravel (CG) 15/25 "SARL MEZIANE";
- Cement "SEG Sour El-Ghozlane."

The proportions of constituents were determined using the Faury method, achieving a 28-day compressive strength exceeding 25 MPa, as detailed in Table 1, where (FCC) indicates the Formulation of Control Concrete.

Table 1. Proportions of concrete constituents for reference (FCC) and sand-excess (FCC + 30% S) mixes

Constituent	FCC (1 m^3)	FCC + 30% S (1 m^3)	FCC (0.05 m^3)	FCC + 30% S (0.05 m^3)
WCS 0/4 (kg)	730	949	36	46.80
FSB (kg)	130	130	7	7
CG 3/8 (kg)	110	110	6	6
CG 8/15 (kg)	455	455	23	23
CG 15/25 (kg)	425	425	21	21
Cement CPJ-CEM II 42.5 (kg)	350	350	17.50	17.50
Mixing Water (L)	180	200	9	10
Water/Cement Ratio	0.51	0.57	0.51	0.57

Seven specimens were fabricated using control concrete dosed at 350 kg/m^3 cement content, alongside seven specimens incorporating a 30% sand excess. All specimens were cast in galvanized metal molds (16 × 32 cm) with standardized vibration to ensure uniformity. Following demolding, the specimens were cured for 28 days under controlled conditions (20°C, 98% relative humidity). Post-curing, surface roughness was eliminated using a Deluxe Hi-Kenma TSURU-TSURU concrete grinder (Fig. 2) to achieve smooth, test-ready surfaces.

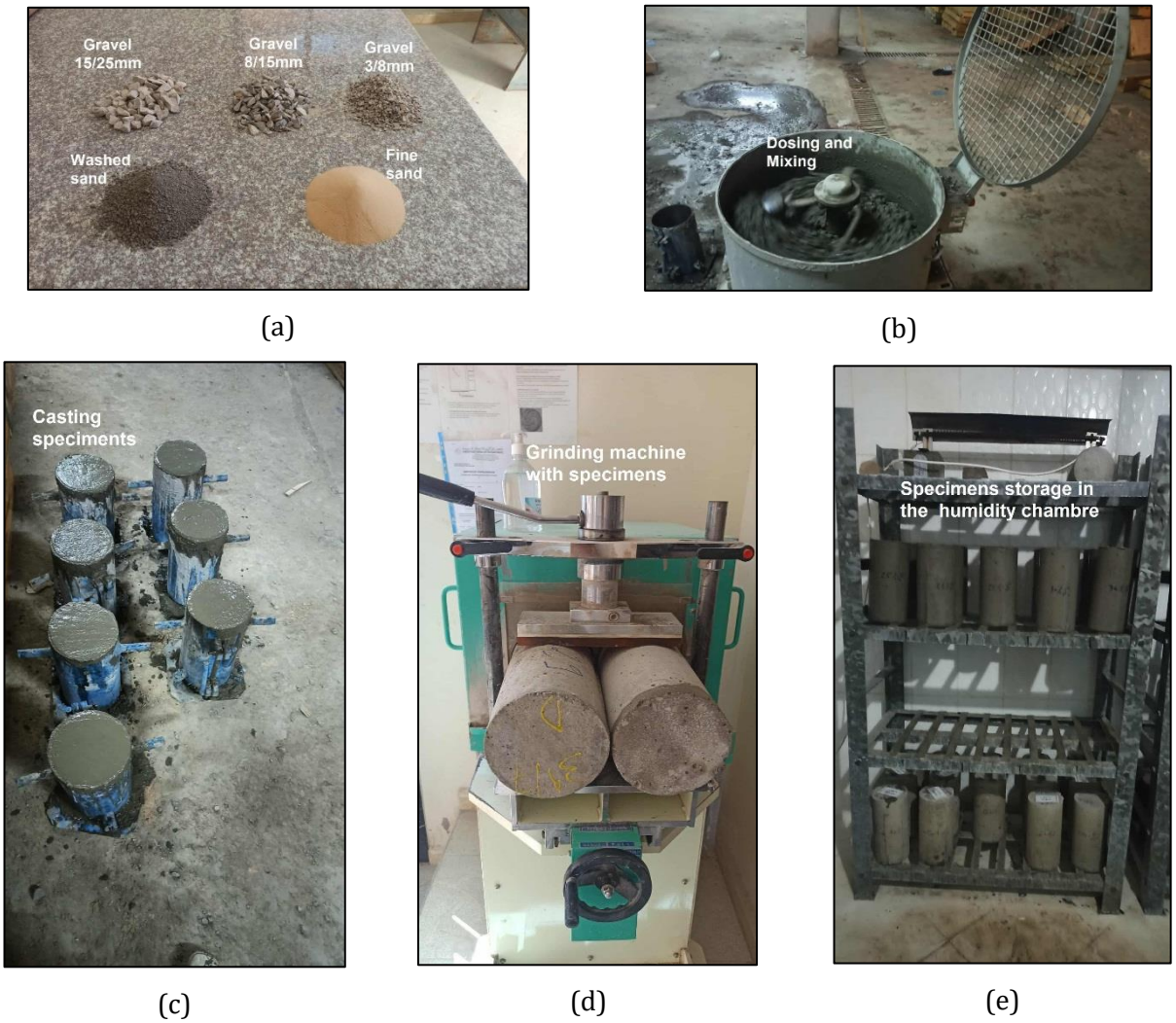

(a) (b)

(c) (d) (e)

Fig. 2. The five stages involved in making and preparing test specimens . (a) selection and preparation, (b) dosing and mixing, (c) pouring, (d) curing, and (e) final grinding

2.2 Preparation of Specimens

In Non-destructive testing (NDT) was performed on the prepared 16 × 32 cm cylindrical specimens [14] using a "Pundit PL-200" ultrasonic device (Fig. 3). The system employs two transducers characterized by a P-wave pulse velocity with a maximum frequency of 54 kHz, operating at pulse speeds of 100–400 Vpp and a pulse echo range of 0.1–1200 µs. Signal acquisition was facilitated by a 7-inch touchscreen (800 × 480 pixels) integrated with a dual-core processor and 8 GB internal memory, ensuring high-resolution waveform visualization.

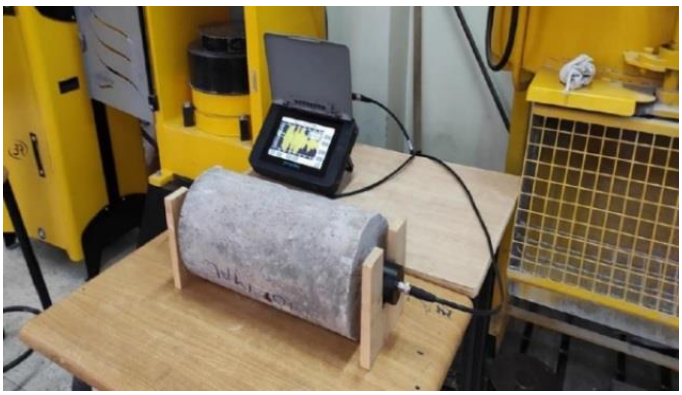

Fig. 3. Longitudinal ultrasonic measurement using the Pundit PL-200 device

The ultrasonic pulse velocity (UPV) method correlates with the material's modulus of elasticity and density; however, its estimation of compressive strength remains approximate due to the absence of a universal physical relationship [15]. Key influencing factors include concrete age, aggregate-to-cement ratio, and moisture content. Higher UPV values indicate superior material quality, reflecting enhanced strength, homogeneity, and density. Transducers were positioned at transverse intervals of 4 cm along the specimen length (yielding 7 signals per specimen) and longitudinally at the specimen ends, centered within 4 cm and 8 cm diameter circles (yielding 3 signals). Testing was conducted on seven control specimens and seven specimens with a 30% sand excess.

2.3 Signal Processing by Multiresolution Analysis Using Wavelets

Multi-resolution analysis (MRA) can be conceptualized as a mathematical framework analogous to observing a signal at varying scales zooming in to resolve fine details and zooming out to capture broader structures [16–18]. Formally, MRA approximates a signal at multiple resolutions through orthogonal projections onto nested subspaces {Vj}, j∈Z. Each approximation at resolution j is governed by a discrete filter that dictates information loss between successive resolutions. A complementary family of subspaces {Wj}, j∈Z. is derived from {Vj}, where Wj represents the orthogonal complement of Vj in Vj−1:

$$Vj - 1 \; = \; Vj \; + \; Wj \; for \; j \; \in \; Z \; with \; Vj \; \perp \; Wj \tag{1}$$

In contrast to {Vj} spaces which are spaces of approximations, {Wj } spaces are spaces of details, so the previous expression can mean that an element of the approximation space of level (j − 1) is decomposed into the approximation of level (j) which is coarser, and the detail of level (j). The wavelet is a finite energy function Ψ:

$$\int_R t^p \Psi(t) dt = 0 \, , \forall \; 0 \leq p \; < n \tag{2}$$

The continuous wavelet transforms of a signal X ∈ L2(R) at time "μ" and scale "s" is defined by:

$$W_X(u,s) = < X, \Psi_{u,s} > = \int_{-\infty}^{+\infty} X(t) \frac{1}{\sqrt{s}} \Psi^* \left(\frac{t-u}{s} \right) dt \tag{3}$$

Where Ψ∗ is the conjugate complex of Ψ. The discrete wavelet transform is then denoted:

$$d_x(j,k) = W_x\left(u = 2^{-j}k, s = 2^{-j}\right), (j,k) \in \; ZxZ \tag{4}$$

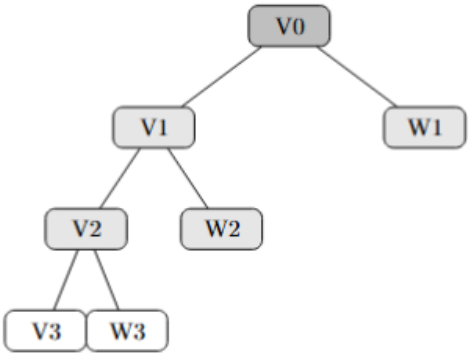

Fig. 4. Schematic of multi-resolution analysis (MRA) illustrating the decomposition of a signal into approximation (*Vj*) and detail (*Wj*) subspaces

The wavelet transform's inherent redundancy is mitigated by constructing an orthonormal basis {ψj,k}(j,k)∈Z for L2(R). Signal decomposition into this basis involves iterative discrete convolutions with low-pass (h) and high-pass filters, followed by decimation (↓2) to retain alternate samples. This

process, implemented via the Mallat algorithm [19], computes approximation and detail coefficients through cascaded filtering and subsampling (Fig. 5).

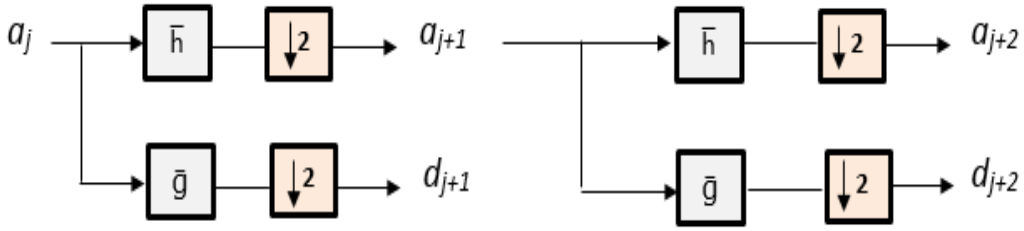

Fig. 5. Signal decomposition workflow using low-pass ($\bar{h}$) and high-pass ($\bar{g}$) filters, with decimation (↓2) at each stage

Daubechies wavelets [20], exemplified by the second-order (N=2) variant (Fig. 6). constitute a family of compactly supported orthogonal wavelets for their balance between localization and smoothness.

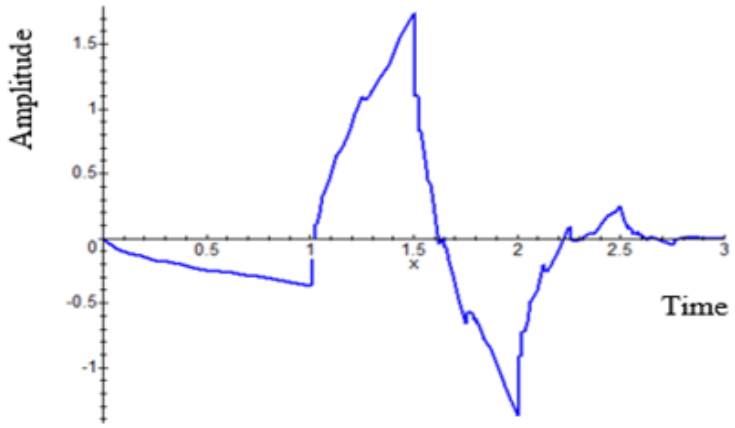

Fig. 6. Daubechies wavelet (order N=2) used for discrete wavelet decomposition

3. Results and Discussions

3.1 Digital Processing of The Database

The analysis of ultrasonic signal distributions between reference and sand-excess concrete reveals distinct patterns critical to defect identification. As illustrated in Fig. 7 reference concrete exhibits a pronounced dominance in signal categories C1–C5, which correspond to baseline amplitudes and noise-free waveforms. This consistency aligns with the homogeneous microstructure and uniform density expected in properly proportioned concrete. In contrast, sand-excess concrete demonstrates a marked shift toward categories C6–C10, characterized by irregular waveforms and elevated amplitudes. These anomalies are attributed to increased porosity and interfacial defects arising from the disproportionate sand content, which disrupts aggregate-cement bonding and introduces microstructural heterogeneity. Further quantification of these trends is provided in Fig. 8, where reference concrete signals in categories C1–C4 constitute over 70% of total occurrences, reflecting stable ultrasonic wave propagation through a cohesive material matrix. Conversely, sand-excess concrete shows a predominance of categories C7–C10, contributing more than 60% of signals. This divergence underscores the sensitivity of ultrasonic testing to compositional deviations, as excess sand alters the material's acoustic impedance and wave attenuation properties.

The observed variability in signal behavior can be contextualized through wavelet analysis. The prominence of C6–C10 categories in sand-excess concrete correlates with high-frequency wavelet coefficients, which capture localized discontinuities such as voids and microcracks. In contrast, the dominance of C1–C5 categories in reference concrete corresponds to low-frequency approximations, indicative of bulk material integrity. This dichotomy validates the utility of multi-resolution analysis in isolating defect-related features from background noise. From a practical perspective, the categorical

shift from C1–C5 to C6–C10 serves as a robust diagnostic marker for sand-related defects. Automated quality control systems leveraging this criterion could flag batches exceeding a 20% contribution from C6–C10 signals, enabling real-time detection of formulation errors. Such an approach reduces reliance on destructive testing while enhancing the scalability of structural health monitoring. The values presented in Table 2 represent mathematical indices extracted from the ultrasonic signal and are specific to the Pundit PL-200 device. These indices were used as reference patterns, and their frequency of occurrence within the measured signal was calculated to assess their repetitiveness.

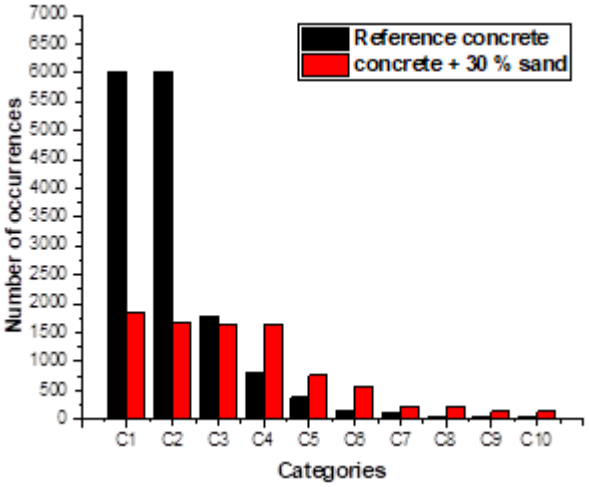

Fig. 7. Distribution of signal value occurrences in reference concrete vs. sand-excess concrete

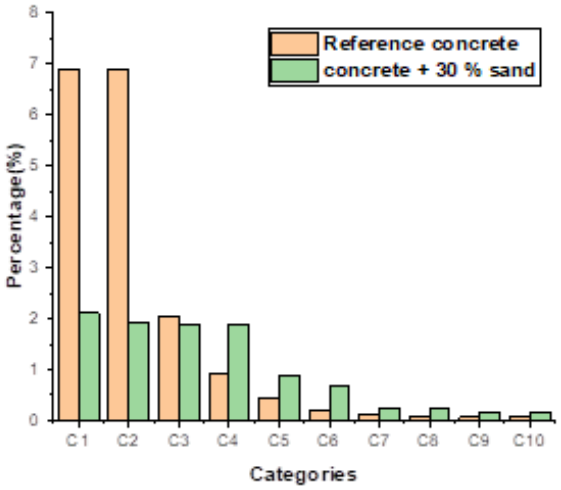

Fig. 8. Percentage contribution of signal categories in reference concrete vs. sand-excess concrete

Table 2. Redundancy statistics for values in the signals studied

CATYGORY	Type of concrete	Value	Number of occurrences	Percentage (%)
CATYGORY1	Reference concrete	32 624	6 020	6.90
	concrete + 30 % sand	47	1 838	2.11
CATYGORY2	Reference concrete	-32 640	6 010	6.89
	concrete + 30 % sand	32 624	1 682	1.93
CATYGORY3	Reference concrete	47	1 794	2.06
	concrete + 30 % sand	-32 640	1 656	1.90
CATYGORY4	Reference concrete	63	797	0.91
	concrete + 30 % sand	31	1 636	1.88
CATYGORY5	Reference concrete	15	381	0.44
	concrete + 30 % sand	63	760	0.87
CATYGORY6	Reference concrete	79	153	0.18

	concrete + 30 % sand	15	576	0.66
CATYGORY7	Reference concrete	0	103	0.12
	concrete + 30 % sand	79	222	0.25
CATYGORY8	Reference concrete	191	54	0.06
	concrete + 30 % sand	0	215	0.25
CATYGORY9	Reference concrete	111	53	0.06
	concrete + 30 % sand	-64	145	0.17
CATYGORY10	Reference concrete	398	52	0.06
	concrete + 30 % sand	127	139	0.16

3.2 Superposition of Ultrasonic Signals

The ultrasonic signals acquired from reference concrete and sand-excess concrete (30% additional sand) were processed using MATLAB software. Amplitude values, extracted from the Proceq PL-Link database, were superimposed to compare longitudinal and transverse waveforms at identical measurement positions. Fig. 9 illustrates the superimposition of signals for both concrete types. A pronounced divergence is observed between the waveforms:

- Longitudinal Signals (Fig. 9a): The reference concrete exhibits a stable, low-amplitude waveform, whereas the sand-excess concrete shows intermittent amplitude spikes and phase shifts.
- Transverse Signals (Fig. 9b): The sand-excess concrete displays reduced signal coherence, with higher attenuation and irregular peaks compared to the reference concrete.

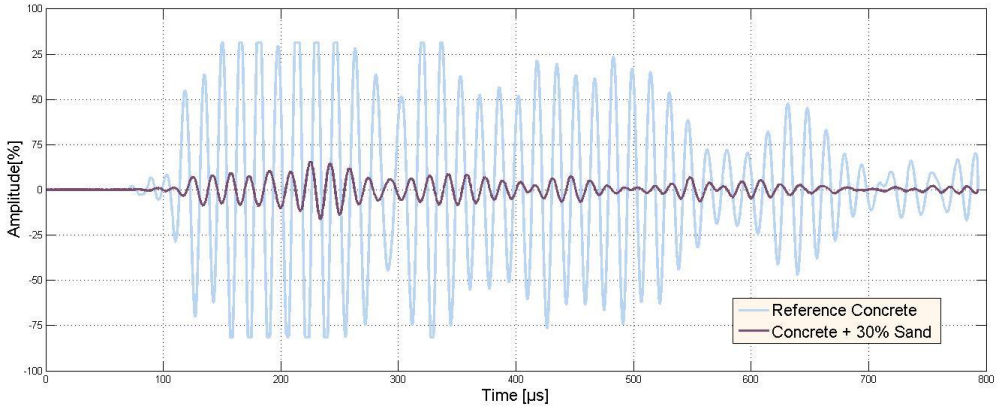

(a)

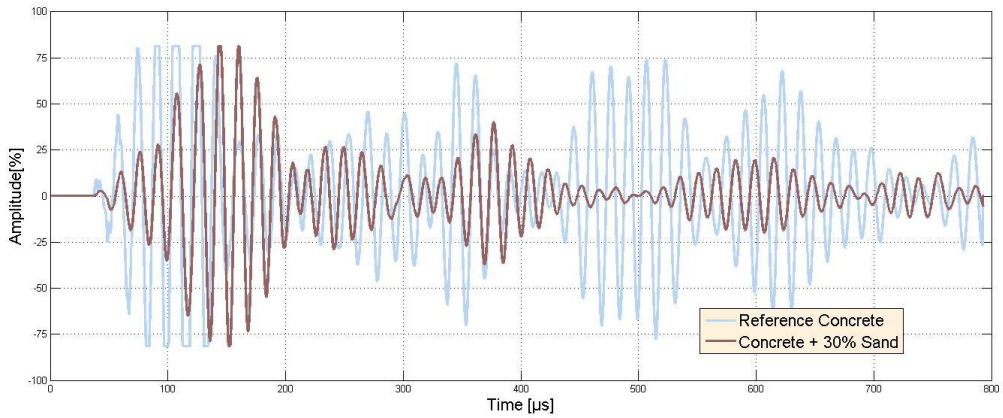

(b)

Fig. 9. Superimposed ultrasonic signals (a) Longitudinal comparison showing amplitude spikes in sand-excess concrete (30% sand), (b) Transverse comparison highlighting signal attenuation in sand-excess concrete (30% sand)

The distinct signal behavior arises from microstructural disparities induced by 30% excess sand. In sand-excess concrete, the overabundance of fine particles disrupts the aggregate-cement matrix,

increasing porosity and creating interfacial voids. These defects scatter ultrasonic waves, manifesting as amplitude spikes (Fig. 9a) and attenuated waveforms (Fig. 9b). Conversely, the homogeneous microstructure of reference concrete facilitates consistent wave propagation, yielding stable signals. The longitudinal signal anomalies (Fig. 9a)) correlate with high-frequency wavelet coefficients, capturing localized voids, while transverse signal attenuation (Fig. 9b) aligns with energy dissipation due to reduced material density.

3.3 Signal Decomposition via Wavelet Analysis

Using the "wavelet toolbox" interface of the "MATLAB" calculation code, we decomposed the signals by using the discrete wavelet transform "DWT" in 04 levels, in this case the second-order Daubechies wavelet, which enabled us to analyse the signals obtained at different scales (resolution). The results of this decomposition are the detail and approximation coefficients, with graphical representations of these coefficients until we obtain the smoothest version of our original signal. This "DWT" transform also enables us to denoise signals characterised by a high level of noise, in order to improve accuracy during information extraction. Analysis of ultrasonic signals decomposed using the Discrete Wavelet Transform (DWT) revealed significant differences between the reference concrete and the concrete with a 30% excess of sand, in both propagation directions (longitudinal and transverse). A detailed interpretation of each decomposition figure is given below:

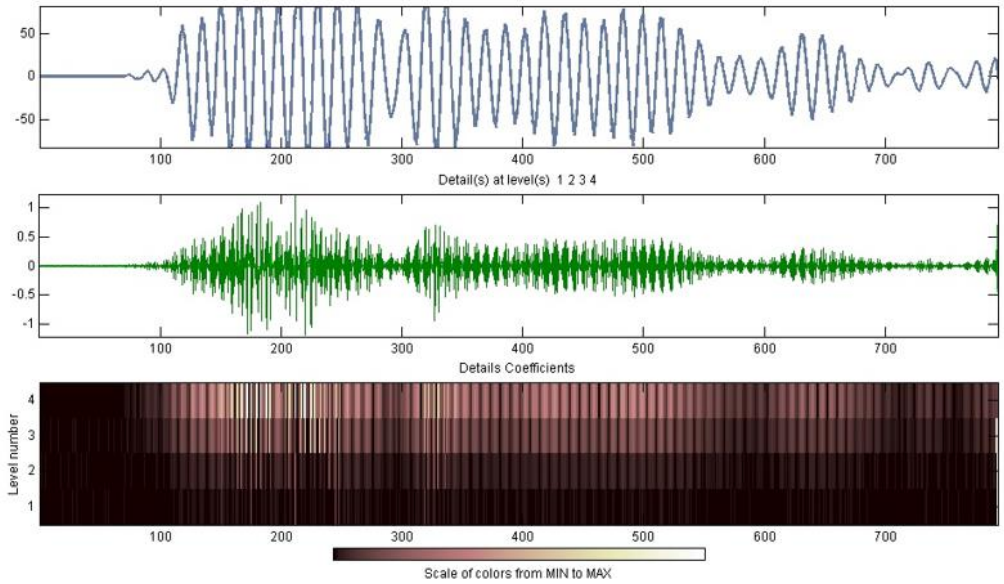

Fig. 10. Longitudinal signal approximation and detail coefficients for reference concrete

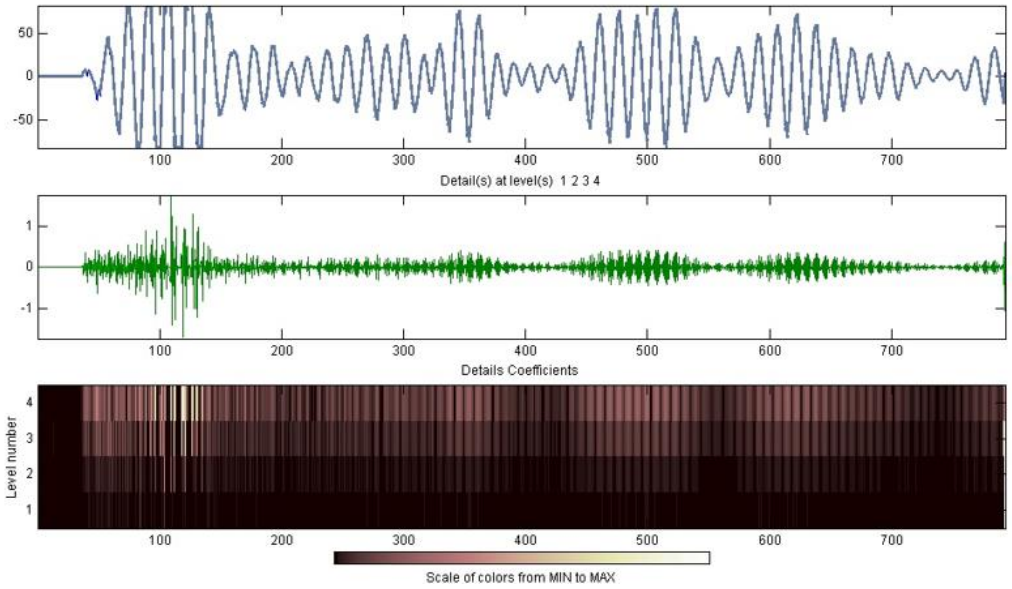

Fig. 11. Transverse signal detail and approximation coefficients for reference concrete

This figure (Fig. 10) shows a clear signal with a regular and well-defined waveform. The detail coefficients from the DWT, especially at levels 1 and 2, are concentrated around the central part of the signal (Time ≈ 200–350 µs), indicating good transmission of ultrasonic energy. The relatively high amplitude and coherent structure suggest that the material is homogeneous and dense, with no major internal disturbances. Compared to the previous figure, In the figure above (Fig. 11), the signal appears slightly more attenuated, which is expected in the transverse direction. However, the waveform remains regular, and the extracted details are well localized, although less intense than in the longitudinal case. The energy is mostly concentrated in the lower detail levels, confirming that the material is healthy, but the transverse direction causes more wave dispersion.

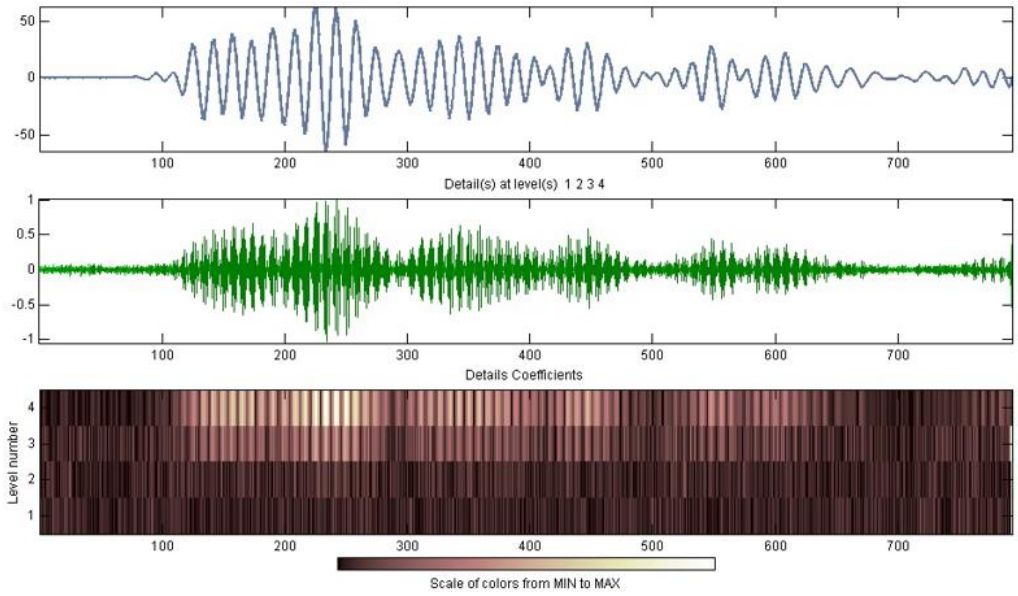

Fig. 12. Longitudinal signal approximation and detail coefficients for sand-excess concrete (30% sand)

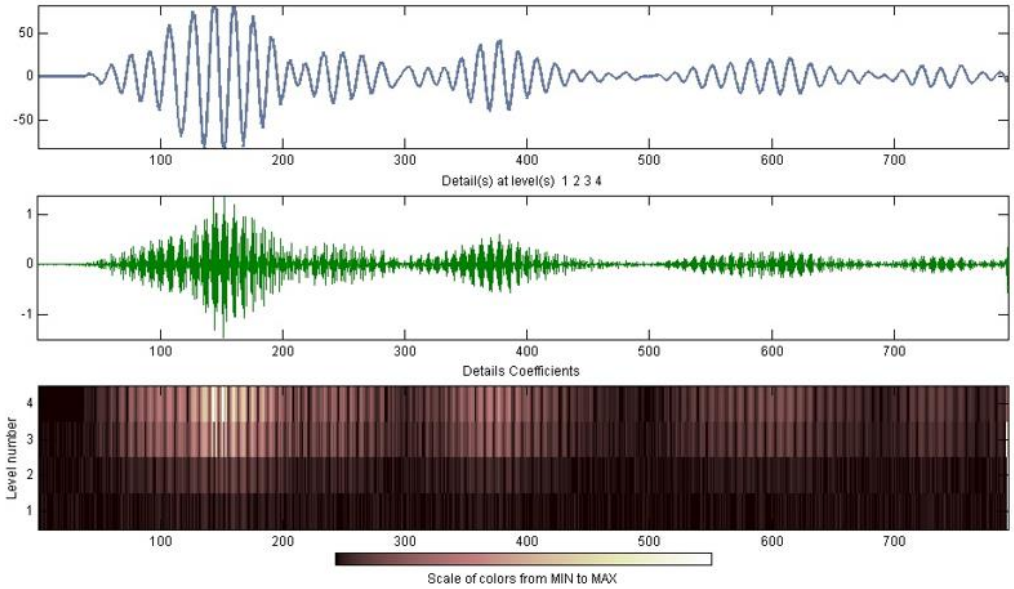

Fig. 13. Transverse signal approximation and detail coefficients for sand-excess concrete (30% sand)

This graphical representation (Fig. 12) shows a noticeable decrease in signal amplitude and a more irregular waveform. The detail coefficients are more spread out, especially from levels 1 to 3. The energy is distributed over a larger portion of the signal, reflecting unstable propagation and the presence of micro-defects. These observations are typical of a heterogeneous concrete, where the excess sand results in poor compaction and multiple interfaces that disturb wave travel.

This illustration (Fig. 13) shows the most pronounced effect of the defect. The signal is strongly attenuated from the beginning, with an asymmetric envelope and lower frequency content. The DWT coefficient distribution shows energy concentrated in a narrow time range (Time ≈ 100–200 μs), followed by a general weakening. This indicates strong energy absorption due to internal heterogeneity and significant scattering. This response is characteristic of a disorganized and porous structure. These observations confirm that excess sand significantly degrades ultrasonic wave transmission, and that this degradation is both visually and quantitatively detectable using the Discrete Wavelet Transform. Each figure clearly demonstrates the ability of this method to reveal the internal structure of concrete, highlighting differences in behavior depending on the propagation direction and the condition of the material.

3.4 Comparative Analysis with Existing Methods

The proposed methodology is contextualized within the broader landscape of wavelet-based signal processing techniques, with key distinctions highlighted against prior studies:

Machorro-Lopez et al. [21] employed continuous wavelet transforms (CWT) with Gaussian wavelets to analyze acoustic emission (AE) signals from concrete beams under flexural loading. Their approach focused on post-processing waveform data to compute wavelet energy (WE) for damage detection, identifying the Gaussian wavelet as optimal for capturing fracture-related features. In contrast, the present study utilizes discrete wavelet transforms (DWT) with Daubechies wavelets, emphasizing compositional defects rather than mechanical damage. By directly comparing decomposition coefficients between reference and sand-excess concrete, this work bypasses the need for energy-based metrics, offering a granular resolution of material heterogeneity.

Hu et al. [22] integrated wavelet packet transforms (WPT) with a hybrid genetic algorithm-backpropagation neural network (GA-BPNN) to classify concrete defects. While their method enhances anomaly detection accuracy through machine learning, it requires extensive training datasets and computational resources. This study, conversely, relies on coefficient-based statistical analysis, enabling defect identification without supervised learning, thus reducing complexity and improving scalability for real-time quality control.

Mousavi et al. [23] applied variational mode decomposition (VMD) to ultrasonic signals from wood samples, targeting physical defects such as voids and decay. Although their work shares a similar non-destructive testing framework, the focus diverges significantly: this research addresses material composition flaws (sand excess) rather than structural voids. The use of DWT here provides a more interpretable decomposition for quantifying constituent-related anomalies, which are less visually apparent than physical discontinuities.

- Methodological Distinction: Unlike CWT/WPT-based studies [21–22], this work leverages DWT's multi-resolution capabilities to isolate compositional defects through coefficient analysis, avoiding reliance on energy thresholds or machine learning.
- Application Scope: Expands ultrasonic testing beyond physical defect detection [23] to diagnose formulation errors, a critical advancement for preemptive quality assurance in concrete production.
- Practical Efficiency: The coefficient-driven approach reduces computational overhead compared to hybrid ML methods [22], aligning with industrial needs for rapid, on-site assessments.

4. Conclusions

This study establishes a wavelet-based framework for non-destructive identification of sand excess defects in concrete, leveraging multi-resolution analysis (MRA) to isolate compositional anomalies. Key findings demonstrate that ultrasonic signal redundancy and distribution patterns serve as robust indicators of material integrity:

- Signal Characterization: The reference concrete exhibited a recurrence of dominant index values (-32, 640, 32, 624), with approximately 70% concentrated within categories C1–C4, indicating a homogeneous microstructure. In contrast, the sand-rich concrete showed repeated values (31, 47), with around 60% falling within categories C7–C10. This distribution is attributed to

increased porosity and interfacial defects resulting from the breakdown of the aggregate–cement bond.

- Wavelet Decomposition: Discrete wavelet transform (DWT) with Daubechies wavelets distinguished defects through approximation coefficients (bulk properties) and detail coefficients (localized voids). Longitudinal signal superimposition revealed amplitude spikes, while transverse analysis highlighted attenuation, correlating with microstructural heterogeneity.
- Methodological Innovation: The coefficient-driven approach eliminates dependency on machine learning, reducing computational complexity and enabling real-time defect detection without extensive training datasets.

Diverging from prior studies focused on physical defects, this work targets formulation errors, advancing ultrasonic testing for preemptive quality control. The integration of MRA enhances sensitivity to subtle compositional deviations, offering a scalable alternative to destructive methods.

Future research should expand the signal database to encompass diverse defect types (aggregate deficiencies, water-cement ratio imbalances) and integrate adaptive algorithms for automated, real-time anomaly classification. Such advancements will further minimize manual intervention, aligning with industrial demands for efficient, high-precision structural.

Acknowledgement

The authors wish to express their gratitude to the team at the LCTP laboratory in Bouira, as well as to the technicians at the Civil Engineering Laboratory of the Faculty of Science and Applied Science at the Akli Mohand Oulhadj University of Bouira, for their support in this study.

References

[1] Rebai B, Benaddi H, Messas T, Salhi M. Evaluation of self-compacting concrete for concrete repair applications. Res. Eng. Struct. Mater., 2025; 11(2): 495-513. http://dx.doi.org/10.17515/resm2024.255st0423rs

[2] Kovler, K., & Roussel, N. (2011). Properties of fresh and hardened concrete. *Cement and Concrete Research*, *41*(7), 775-792. https://doi.org/10.1016/j.cemconres.2011.03.009

[3] Pedram, M., Taylor, S., Hamill, G., Robinson, D., OBrien, E. J., & Uddin, N. (2022). Experimental evaluation of heat transition mechanism in concrete with subsurface defects using infrared thermography. *Construction and Building Materials*, *360*, 129531. https://doi.org/10.1016/j.conbuildmat.2022.129531

[4] Joshaghani, A., & Shokrabadi, M. (2022). Ground penetrating radar (GPR) applications in concrete pavements. *International Journal of Pavement Engineering*, *23*(13), 4504-4531. https://doi.org/10.1080/10298436.2021.1954182

[5] Schabowicz, K. (2019). Non-destructive testing of materials in civil engineering. *Materials*, *12*(19), 3237. https://doi.org/10.3390/ma12193237

[6] Lin, Y., Lai, C. P., & Yen, T. (2003). Prediction of ultrasonic pulse velocity (UPV) in concrete. *Materials Journal*, *100*(1), 21-28. DOI: 10.14359/12459

[7] Kogbara, R. B., Iyengar, S. R., Grasley, Z. C., Masad, E. A., & Zollinger, D. G. (2015). Non-destructive evaluation of concrete mixtures for direct LNG containment. *Materials & Design*, *82*, 260-272. https://doi.org/10.1016/j.matdes.2015.05.084

[8] Ouahabi A. Digital signal and image processing series. Signal and image multiresolution analysis, 1st edition, London John Wiley-ISTE, 2012, ISBN 978-1848212572.

[9] Arbaoui, A., Ouahabi, A., Jacques, S., & Hamiane, M. (2021). Concrete cracks detection and monitoring using deep learning-based multiresolution analysis. *Electronics*, *10*(15), 1772. https://doi.org/10.3390/electronics10151772

[10] Guo, T., Zhang, T., Lim, E., Lopez-Benitez, M., Ma, F., & Yu, L. (2022). A review of wavelet analysis and its applications: Challenges and opportunities. *IEEe Access*, *10*, 58869-58903. https://doi.org/10.1109/ACCESS.2022.3179517

[11] Arbaoui, A., Ouahabi, A., Jacques, S., & Hamiane, M. (2021). Wavelet-based multiresolution analysis coupled with deep learning to efficiently monitor cracks in concrete. *Frattura ed Integrità Strutturale/Fracture and Structural Integrity*, *15*(58), 33-47. https://doi.org/10.3221/IGF-ESIS.58.03

[12] Testing hardened concrete - Part 1: Shape, dimensions and other requirements for test specimens and moulds. Standard EN 12390-1, (October 2001).

[13] Testing Hardened Concrete — Part 2: Making and Curing Specimens for Strength Tests. Standard EN 12390-2, (October 2001).

[14] Testing concrete in structures — Part 4: Determination of ultrasonic pulse velocity. Standard EN 12504-4, (July 2021).
[15] Charbit M, Blanchet G. Digital signal and image processing series. Digital signal and image processing using MATLAB, Volume 1: Fundamentals, 2nd Edition, London John Wiley-ISTE, July 2014, ISBN 978-1-118-99957-8.
[16] Hashmi, A. F., Shariq, M., & Baqi, A. (2022). Age-dependent strength assessment of low calcium fly ash concrete based on ultrasonic pulse velocity and rebound hammer number measurement. *Iranian Journal of Science and Technology, Transactions of Civil Engineering*, *46*(6), 4327-4341. https://doi.org/10.1007/s40996-022-00905-x
[17] OUAHABI A. traité signal et Image. Analyse Multirésolution pour le Signal et l'Image, IC2, Lavoisier Paris, 2012 : 35-46 , ISBN 978-2-7462-2394-3.
[18] Kang, L., Liu, G., Huang, J., & Li, J. (2022). Super-resolution method for MR images based on multi-resolution CNN. *Biomedical Signal Processing and Control*, *72*, 103372. https://doi.org/10.1016/j.bspc.2021.103372
[19] Arbaoui, A., Aribi, C., Boumaiza, M., Mohamadi, S., & Ait Ahmed, F. (2022, May). CNN-Based Concrete Cracks Detection Using Multiresolution Analysis. In *2022 7th International Conference on Image and Signal Processing and their Applications (ISPA)* (pp. 1-5). IEEE. https://doi.org/10.1109/ISPA54004.2022.9786328
[20] Luo, D., Li, Y., Luo, Z., & Han, C. (2023, July). Detection and analysis of hanging basket wire rope broken strands based on Mallat algorithm. In *International Conference on Neural Computing for Advanced Applications* (pp. 518-532). Singapore: Springer Nature Singapore. DOI: https://doi.org/10.1007/978-981-99-5844-3_38
[21] Mandala, S., Pratiwi Wibowo, A. R., Adiwijaya, Suyanto, Zahid, M. S. M., & Rizal, A. (2023). The effects of Daubechies wavelet basis function (DWBF) and decomposition level on the performance of artificial intelligence-based atrial fibrillation (AF) detection based on electrocardiogram (ECG) signals. *Applied Sciences*, *13*(5), 3036. https://doi.org/10.3390/app13053036
[22] Machorro-Lopez, J. M., Hernandez-Figueroa, J. A., Carrion-Viramontes, F. J., Amezquita-Sanchez, J. P., Valtierra-Rodriguez, M., Crespo-Sanchez, S. E., ... & Martinez-Trujano, L. A. (2023). Analysis of acoustic emission signals processed with wavelet transform for structural damage detection in concrete beams. *Mathematics*, *11*(3), 719. https://doi.org/10.3390/math11030719
[23] Hu, T., Zhao, J., Zheng, R., Wang, P., Li, X., & Zhang, Q. (2021). Ultrasonic based concrete defects identification via wavelet packet transform and GA-BP neural network. *PeerJ Computer Science*, *7*, e635. https://doi.org/10.7717/peerj-cs.635
[24] Mousavi, M., Taskhiri, M. S., & Gandomi, A. H. (2023). Standing tree health assessment using contact–ultrasonic testing and machine learning. *Computers and Electronics in Agriculture*, *209*, 107816. https://doi.org/10.1016/j.compag.2023.107816
[25] Amriou, A., et al. (2022). Effect of Gravel Content on Mechanical Performance and Porous Structure of Concrete. *Annales De Chimie-Science Des Materiaux, 46*(1), 19–25. https://doi.org/10.18280/acsm.460103.
[26] Borisiuk, E., & Kochenkova, E. (2022). An Effect of Sands of Different Grades on Structural and Mechanical Properties of Sand Concrete. *Solid State Phenomena, 335*, 151–157. https://doi.org/10.4028/p-8n0znm
[27] Lee, M. (2022). Concrete durability problems: physicochemical and transport mechanisms. *Elsevier eBooks*, 69–107. https://doi.org/10.1016/b978-0-12-824354-1.00003-9
[28] Sahni, H., & Bashar, N. (2024). Mechanical and durability characteristics of concrete utilizing waste foundry sand. *International Journal of Research in Engineering and Innovation, 8*(3), 114–119. https://doi.org/10.36037/ijrei.2024.8303
[29] Jadhav, A., et al. (2024). Influence of river sand and crushed sand on strength gain for M30 concrete. Futuristic Trends in Construction Materials & Civil Engineering Volume 3 Book 4. 2024; 3: 49-59. https://doi.org/10.58532/v3bice4p4ch1
[30] Chitour M, Khadraoui F, Mansouri K, Rebai B, Menasria A, Zemmouri A, Touati S, Boumediri H. A novel high order theory for static bending of functionally graded (FG) beams subjected to various mechanical loads. Res. Eng. Struct. Mater., 2024; 10(4): 1523-1539. http://dx.doi.org/10.17515/resm2024.141me0104rs
[31] Boutrid, A., Rebai, B., Mamen, B., Bouhadra, A., & Tounsi, A. (2024). Combined effect of temperature dependent material properties and boundary conditions on non-linear thermal stability of porous FG beams. *Acta Mechanica*, *235*(5), 2867-2887. https://doi.org/10.1007/s00707-024-03860-y
[32] Messas, T., Rebai, B., Mansouri, K., Chitour, M., Berkia, A., & Litouche, B. (2023). Analyzing vibration behavior of nano FGM (Si3N4/SUS304) plates: impact of homogenization models and nano parameters. J. Nano-Electron. Phys. 15 No 6, 06018 (2023). DOI: https://doi.org/10.21272/jnep.15(6).06018